AIAA SciTech Forum
8–12 January 2024, Orlando, FL
AIAA SCITECH 2024 Forum

PREPRINT

Controller Agnostic Design Metrics for Stochastic Disturbance Rejection

Bernardo Bahia Monteiro,* Ilya Kolmanovsky,† and Carlos E. S. Cesnik‡
University of Michigan, Ann Arbor, MI 48109

This paper presents a framework to compute the probabilities and the expected frequencies of exceedance of design limits by the outputs and inputs of a linear system driven by Gaussian noise. It is assumed that the system has a second input that can be used for feedback control based on the measurements of one of the outputs. This approach is able to capture the effects of the controller by assuming a shape for the loop sensitivity function, which must respect the Bode integral relation. For illustration, a surrogate model of a supersonic aircraft configuration in the approach-to-land flight phase is considered, and the probabilities and expected frequencies of exceedance of design limits of angle of attack, glideslope deviation, elevator deflection, and elevator deflection rate are calculated. To enable fast and accurate derivative computation for gradient-based optimization, frequently used in large-scale multidisciplinary design optimization (MDO), the derivatives of these quantities with respect to design parameters are derived analytically. They are verified against a finite difference approximation with excellent agreement. A simple optimization problem for designing the sensitivity function is considered and the resulting closed-loop system is analyzed.

I. Introduction

Accounting for gusts is an essential part of aircraft design. It is important for structural sizing (14 CFR 25.341), as well as for passenger and crew safety and comfort. Turbulence-related accidents were the most frequent accident type in both 2021 and 2022, and accounted for more than one-third of all accidents involving U.S. scheduled airline flights in the 2009 to 2018 period, resulting in serious injury to passengers and/or crew members [1]. The lack of fatal accidents in recent years attests to the progress made in the technologies and requirements for considering gusts in the aircraft design process.

One particular situation where gust disturbances are a critical factor in guaranteeing the safety of new aircraft designs is the low-speed flight phases of commercial supersonic aircraft. This type of aircraft has received renewed attention in recent years due to the development of new technology that reduces the loudness of the sonic boom, thereby promising to enable supersonic flight over land (see e.g., [2] and references therein). The culmination of these efforts is the design and fabrication of the X-59 low-boom supersonic aircraft demonstrator, which NASA is planning to fly over U.S. communities, starting in 2024, to evaluate the public's response to the improved sonic-boom signature [3, 4]. However, to be viable and certifiable, a supersonic aircraft must also operate satisfactorily at low-speed flight conditions, especially during take-off, initial climbing, final approach, and landing. These flight regimes are very different from the supersonic cruise for which these aircraft are usually optimized, and, due to the lower altitude, while flying in these conditions the aircraft is more susceptible to weather phenomena such as gusts.

Gusts are usually modeled as either discrete gusts (usually of the one-minus-cosine type) or continuous gusts (i.e., turbulence), in which case they are idealized as (locally) stationary Gaussian stochastic processes [5]. In the latter case, the gusts are fully described by their power spectral density (PSD), and the most commonly used models are the Dryden [6], von Kármán [7], Kaimal [8], and Mann [9] models. Since the introduction of the power spectral method applied to gusts in 1952–1953, the stochastic modeling has gained wide acceptance [10] even though this approximation was found to yield non-conservative results in some cases [11]. For this reason, it did not supersede the older discrete gust certification requirements (14 CFR 25.341(a)). In any case, the stochastic modeling of gusts has been well validated in practice and is enshrined in the certification procedure for aircraft (14 CFR 25.341(b)) and wind turbines (IEC 61400-1). Furthermore, Gaussian processes have been extensively studied in the mathematical literature and offer a very

*PhD Candidate, Department of Aerospace Engineering, bbahia@umich.edu, AIAA Member.
†Pierre T. Kabamba Collegiate Professor, Department of Aerospace Engineering, ilya@umich.edu, AIAA Associate Fellow.
‡Richard A. Auhll Department Chair, Clarence L. "Kelly" Johnson Collegiate Professor, Department of Aerospace Engineering, cesnik@umich.edu, AIAA Fellow.

tractable framework, both in the time and in the frequency domains, which is not the case for the more recent and much more computationally expensive models based on large-eddy simulations [12–14].

The modeling of gusts as Gaussian processes, however, poses a dilemma because it makes it mathematically impossible to guarantee that the aircraft can reject all gusts it encounters with probability one. This is because Gaussian processes have unbounded support, meaning they can take any real value with a probability greater than zero. In the linear setting that is traditionally used for analyzing the aircraft responses under Gaussian turbulence, these responses (e.g., pitch angle, load factor, etc.) will also be Gaussian processes. Therefore, the probability of them exceeding any limit imposed by the design is greater than zero. A statistical approach must then be employed and was developed to allow the inclusion of this method in the certification requirements.

For the certification of transport aircraft, 14 CFR 25.341(b) Continuous Turbulence Design Criteria requires that the root-mean-square (RMS) value of the gust loads resulting from normalized von Kármán turbulence multiplied by a turbulence intensity specified by the regulation stays below the limit load for the design. As documented in Hoblit [10] and in AC 25.341-1, this value can be interpreted as the RMS gust velocity multiplied by the gust loads peak-to-RMS ratio, that is, the number of standard deviations that the peak gust load is away from the RMS gust load. This requirement is equivalent to ensuring that the load does not exceed the limit load with some preestablished instantaneous probability, which is also known in the literature as a *chance constraint* [15].

The instantaneous probability of exceedance is related to the measure of the trajectories outside of the allowable limits, which, if the process is ergodic, is equal to the proportion of time spent outside the limits [16]. Due to the nonlinearity present in real systems, it might not be possible to recover from an exceedance event (e.g., low altitude stall, loss of control, etc.), so, in addition to requiring the probability of such events to be small, it is also desirable that they happen with low frequency. It is worth noting that these nonlinearities are very complicated in their own right. For example, stall is a dynamic effect [17] thus it does not happen instantaneously after the critical angle of attack is crossed.

The expected frequency of exceedance (or upcrossings) of design limits by a random process can be evaluated using Kac-Rice's formula [18, 19], and it provides more information about the likelihood of an exceedance event. In fact, since the point process of upcrossings of increasingly high levels by a stochastic process with finite covariance converges to a Poisson process with a rate given by the expected frequency of upcrossings [20], this frequency can be used to estimate the joint probability of exceedance, that is, the probability of exceeding a specified level in a period of time, e.g., the lifetime of the aircraft.

The instantaneous probability and expected frequency of exceedance metrics have been previously considered as safety metrics for airplane flight in turbulence by Richardson et al. [21, 22]. They proposed the concept of a "stationary flight envelope," that is, a subset of the usual flight envelope in which an aircraft flying under stochastic gust conditions is guaranteed to be able to maintain steady flight within a certain risk level defined by one of these metrics. These same ideas can be applied to the landing flight phase, but, for this, the closed-loop effects of having a pilot/controller must be considered.

Traditionally, complex systems such as aircraft are designed using a sequential strategy that simplifies the dependence between different engineering disciplines, allowing them to be addressed both independently and consecutively. The controller design is usually done at the end of this sequential process, when the plant is fully defined and, consequently, resources are committed to its manufacture, making changes in the plant design very costly [23]. For instance, in the case of aircraft design, the airframe necessitates specialized tooling and jigs to be manufactured, and it is therefore very expensive to alter the design once production starts. On the other hand, the control algorithms consist of software, which can be efficiently changed and adjusted as far in the design cycle as in-flight testing (e.g., [24]) as well as during the life cycle of the aircraft.

This sequencing is desirable for the reasons aforementioned. However, being able to obtain closed-loop metrics of the design early in the design process that can promote the controllability of the vehicle later on can be a game changer. This is the case, for example, when designing an aircraft with maneuver load alleviation (MLA) or gust load alleviation (GLA) systems, since the presence of those systems allows for weight savings in the structure if designed accordingly. The inclusion of the control discipline in the design process can be made naturally in the framework of multidisciplinary design optimization (MDO) [25].

When control design is considered within an MDO setting, it is usually based in uses simpler control design methods than the ones used when designing only the controller but not the plant. For example, in the related problem of GLA, flap deflection scheduling [26], linear quadratic [27], proportional integral [28], and static output feedback [29] control design techniques were used when designing the control system at the same time as the plant, while linear quadratic Gaussian [30–32], adaptive feedforward [33], model predictive control [34, 35], and H_2/H_∞ [36, 37] controllers were proposed for sequential design. The case of designing an autoland control is even more complex due to the presence of

multiple phases (glide-slope/localizer acquisition and tracking, flare and align) [38]. This motivates the search for an approach to calculate a bound for the performance of the closed-loop system without a fully-fledged controller design, which we refer to as a *controller agnostic approach*. This approach starts by assuming the existence of a well-designed controller and tries to find the limitations of its performance when combined with the plant. The plant is then designed assuming closed-loop performance at the limits of achievable performance and the detailed control design is left to later in the design cycle. This approach was previously explored by the authors for the case of MLA [39] and GLA [40].

One controller agnostic approach for evaluating the gust disturbance rejection of supersonic configuration aircraft flying at low speeds was considered by Cunis et al. [41] using ideas from optimal control such as reachable sets. Their framework allows for nonlinear dynamics and efficient calculation of derivatives with respect to design variables but requires solving an optimal control suboptimization problem, which is a computationally costly task. Furthermore, due to the time-domain approach, sampling schemes had to be used to deal with continuous gust [42], which further increases the computational cost.

The present paper introduces an alternative approach that is also controller agnostic but in the frequency domain. The aircraft is assumed to have an active controller, and the impact of this controller on the design is assessed via the design of the closed-loop sensitivity function [43]. Specifically, the paper examines the probability and the expected frequency of exceedance of design limits for flight-path deviation, angle of attack, control deflection, and control deflection rate of a linearized aircraft model around a nonlinear trim point. The Bode integral relation [44, 45], a fundamental result of control theory, is enforced on the sensitivity function, as well as robust S-based disk margins, which bound the classical gain and phase margins [46]. The derivatives of these metrics with respect to the design variables are calculated analytically, allowing their inclusion as constraints in large-scale MDO [47, 48]. The metrics are then applied to a longitudinal flight dynamics model of the University of Washington's Supersonic Configurations at Low Speeds (SCALOS) model [49–54], using the parameterized surrogate aerodynamic model developed by Guimarães et al. [55].

This paper is organized as follows: Section II introduces the proposed metrics and the theory employed for their calculation; Section III presents the aircraft model used to prototype the metric, as well as the proposed parameterization for the sensitivity function; and Section IV presents the resulting metrics and their sensitivities from applying the proposed methodology to that aircraft model. Finally, Section V provides some concluding remarks for this study.

II. Theoretical Formulation

A. Computation of the probability of exceedance and expected frequency of exceedance metrics

In this paper, the disturbance rejection capability of the closed-loop system is accessed. The plant, shown in Figure 1, is assumed to be linearized around an operating point and to have two inputs, namely one disturbance input (d) and one control input (u), and two outputs, from which one (y) is used for feedback, and the other (z) is purely a performance metric that is not used for feedback. It is assumed that the disturbance input is Gaussian and stationary.

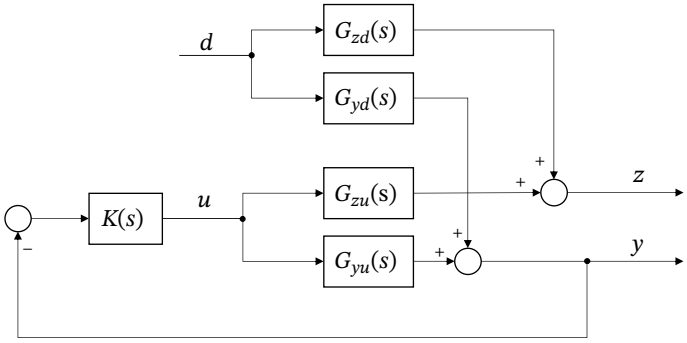

Fig. 1 Plant with two inputs (d, u) and two outputs (y, z), with a feedback loop with a controller $K(s)$ between y and u.

The plant is assumed to have a state space representation given by

$$\begin{aligned} \dot{\boldsymbol{x}} &= \boldsymbol{A}\boldsymbol{x} + \boldsymbol{B_u}u + \boldsymbol{B_d}d \\ \begin{bmatrix} y \\ z \end{bmatrix} &= \begin{bmatrix} \boldsymbol{C_y} \\ \boldsymbol{C_z} \end{bmatrix} \boldsymbol{x} + \begin{bmatrix} D_{yu} & D_{yd} \\ D_{zu} & D_{zd} \end{bmatrix} \begin{bmatrix} u \\ d \end{bmatrix} \end{aligned} \tag{1}$$

from which the transfer functions shown in Figure 1 can be extracted:

$$G_{yd}(s) = \boldsymbol{C_y}(s\boldsymbol{I} - \boldsymbol{A})^{-1}\boldsymbol{B_d} + D_{yd} \tag{2a}$$
$$G_{zd}(s) = \boldsymbol{C_z}(s\boldsymbol{I} - \boldsymbol{A})^{-1}\boldsymbol{B_d} + D_{zd} \tag{2b}$$
$$G_{yu}(s) = \boldsymbol{C_y}(s\boldsymbol{I} - \boldsymbol{A})^{-1}\boldsymbol{B_u} + D_{yu} \tag{2c}$$
$$G_{zu}(s) = \boldsymbol{C_z}(s\boldsymbol{I} - \boldsymbol{A})^{-1}\boldsymbol{B_u} + D_{zu} \tag{2d}$$

Following the controller agnostic approach, the controller $K(s)$ is not designed but instead the sensitivity function of the output used for feedback, i.e.,

$$S(s) = (1 + G_{yu}(s)K(s))^{-1} \tag{3}$$

is considered as a design variable, and a suitable parameterization has to be chosen, such as the one proposed in Section III.C. The closed-loop transfer functions can then be expressed in terms of the open-loop transfer functions (2) and the sensitivity function (3):

$$H_{yd}(s) = S(s)G_{yd}(s) \tag{4a}$$
$$H_{ud}(s) = G_{yu}^{-1}(s)[S(s) - 1]G_{yd}(s) \tag{4b}$$
$$H_{zd}(s) = G_{zd} + G_{zu}(s)G_{yu}^{-1}(s)[S(s) - 1]G_{yd}(s) \tag{4c}$$

Due to the involved transfer functions being linear-time-invariant, the outputs of the system will also be Gaussian and stationary, and their PSDs can be readily computed, including the PSD of the rate of the control action, $\dot{u}$:

$$\Phi_y(\omega) = |H_{yd}(j\omega)|^2\Phi_d(\omega) \tag{5a}$$
$$\Phi_z(\omega) = |H_{zd}(j\omega)|^2\Phi_d(\omega) \tag{5b}$$
$$\Phi_u(\omega) = |H_{ud}(j\omega)|^2\Phi_d(\omega) \tag{5c}$$
$$\Phi_{\dot{u}}(\omega) = \omega^2|H_{ud}(j\omega)|^2\Phi_d(\omega) \tag{5d}$$

where $\Phi_d(\omega)$ denotes the PSD of the disturbance, e.g., the von Kármán turbulence spectrum.

The probability of exceedance and the expected frequency of exceedance are functions of the moments of their PSDs, defined as follows.

Definition 1. The m-th spectral moment of a stationary stochastic process $\{\xi(t); t \geq 0\}$ with PSD $\Phi_\xi(\omega)$ is defined as

$$\lambda_\xi^m = \int_0^\infty \omega^m \Phi_\xi(\omega)\,\mathrm{d}\omega \qquad m = 0, 1, \ldots$$

For a general dynamical system, these moments can be calculated by three approaches: (i) direct integration of the PSD in the frequency domain; (ii) solution of a Lyapunov equation on the state space matrices (e.g., [56]); (iii) time domain simulation and integration of the autocovariance function.

For the sensitivity function approach, the direct integration of the PSD is more suitable because, in addition to it being a frequency domain approach, it requires the inversion of some transfer functions, namely the transfer function from the control action to the output used for feedback. This inverse transfer function is in general non-causal (relative degree less than zero), and therefore it does not admit a space-state representation.

The convergence of the integral depends on both the relative degree of the closed loop transfer function and the decay of the disturbance PSD at high frequencies. In particular, since the von Kármán spectrum has a power law decay at high frequencies with exponent $-\frac{5}{3}$, and the zeroth and second moments of the PSDs are to be computed, it is required that all closed-loop transfer functions have a relative degree of at least two. This is discussed by Hoblit [10, Appendix E].

The probability of exceedance can be calculated using the following result from random process theory:

Fact 2. The probability that the stationary Gaussian process $\{\xi(t); t \geq 0\}$, with mean μ_ξ and zeroth spectral moment λ_ξ^0 exceeds the level L is

$$\mathbb{P}\{\xi > L\} = \frac{1}{2} - \operatorname{erf}\left(\frac{L - \mu_\xi}{\lambda_\xi^0 \sqrt{2}/(2\pi)}\right)$$

where erf denotes the error function, i.e., $\operatorname{erf} z = \frac{2}{\sqrt{\pi}} \int_0^z e^{-\tau^2} \, \mathrm{d}\tau$.

Note that the 2π factor from the denominator comes from the definition of the Fourier transform used to make it compatible with the Laplace transform. Specifically, the PSD, $\Phi_\xi(\omega)$, and the autocovariance, $R_\xi(\tau)$, functions of any stationary random process $\xi(t)$ form a Fourier transform pair, and we use the convention that

$$\Phi_\xi(\omega) = \int_0^\infty R_\xi(\tau) e^{-j\omega\tau} \, \mathrm{d}\tau \tag{6}$$

$$R_\xi(\tau) = \frac{1}{2\pi} \int_0^\infty \Phi_\xi(\omega) e^{j\omega\tau} \, \mathrm{d}\omega \tag{7}$$

If $\xi(t)$ must be constrained to the interval $[L^-, L^+]$, $L^- \leq L^+$, then the probability of it exiting that interval can be obtained by simple sum, i.e., $\mathbb{P}(\{\xi < L^-\} \cup \{\xi > L^+\}) = \mathbb{P}\{\xi < L^-\} + \mathbb{P}\{\xi > L^+\}$, since the involved intervals are disjoint.

Next, we proceed by defining an upcrossing and stating the formula for calculating the expected frequency of exceedance (i.e., the expected frequency of upcrossings) of a level L by a stationary Gaussian random process. We follow the treatment by Leadbetter et al. [20].

Definition 3. Let $\mathcal{G}_L \subset C^0(\mathbb{R}_+ \longrightarrow \mathbb{R})$ denote the class of continuous functions that are not identically equal to $L \in \mathbb{R}$ in any subinterval of the real line, i.e.,

$$\mathcal{G}_L = \{f \in C^0(\mathbb{R}_+ \longrightarrow \mathbb{R}) : f(t) \neq L \text{ for some } t \in (a, b) \text{ and for all } (a, b) \subseteq \mathbb{R}_+\}.$$

A function $f \in \mathcal{G}_L$ is said to have a *strict upcrossing* of the level L at the point t_0 if for some $\varepsilon > 0$, $f(t) \leq L$ for all $t \in [t_0 - \varepsilon, t_0]$ and $f(t) \geq L$ for all $t \in [t_0, t_0 + \varepsilon]$

Fact 4. Consider a strictly stationary random process $\{\xi(t) : t \geq 0\}$ with continuous cumulative distribution function. Then all sample paths of ξ are members of $\mathcal{G}_L$ with probability one.

Definition 5. Let $N^+_{L,(t_0,t_1)}(\xi)$ denote the number of upcrossings of the level L by the strictly stationary random process with continuous cumulative distribution function $\{\xi(t) : t \geq 0\}$ in the interval (t_0, t_1).

The *expected frequency of exceedance* of a level L by ξ is defined as the expected number of upcrossings of L in unit time and is denoted as $\mathbb{E}[N^+_L(\xi)]$ (the interval subscript is dropped), i.e.,

$$\mathbb{E}[N^+_L(\xi)] = \mathbb{E}[N^+_{L,(\tau,\tau+1)}(\xi)].$$

Note that, since $\xi(t)$ is stationary, this value is independent of the choice of τ.

Fact 6. (Kac-Rice's formula) [18, 19] Let $\{\xi(t), t \geq 0\}$ be a strictly stationary normal random process with mean μ and finite second moment. Then the frequency of upcrossings of the mean can be calculated as

$$\mathbb{E}[N^+_\mu(\xi)] = \frac{1}{2\pi} \sqrt{\frac{\lambda_\xi^2}{\lambda_\xi^0}}$$

and the expected frequency of exceedance of an arbitrary constant level L is given by

$$\mathbb{E}[N^+_L(\xi)] = \mathbb{E}[N^+_\mu(\xi)] \exp\left[-\frac{1}{2} \frac{(L - \mu)^2}{\lambda_\xi^0/(2\pi)}\right]$$

Due to the linearity of the expectation operator, the expected frequency of exiting an interval $[L^-, L^+]$, $L^- \leq L^+$ can be obtained by summing the frequency of upcrossing of the higher limit and the frequency of downcrossings of the lower limit, i.e.,

$$\mathbb{E}[N^+_{L^+}(\xi) + N^-_{L^-}(\xi)] = \mathbb{E}[N^+_{L^+}(\xi)] + \mathbb{E}[N^-_{L^-}(\xi)] = \mathbb{E}[N^+_{L^+}(\xi)] + \mathbb{E}[N^+_{-L^-}(-\xi)] \tag{8}$$

B. Derivatives of PSD moments with respect to state space matrices

To enable gradient-based optimization, it is important to have an efficient way to compute the derivatives of the functions of interest. In particular, the probability of exceedance and the expected frequency of exceedance of y, z, u, and $\dot{u}$ are simple functions of the zeroth and second moments of the PSDs of y, z, u and of the second and fourth moments of u, respectively. The derivatives of these moments with respect to the state-space matrices are calculated as shown next, and they can be integrated into an MDO problem using the chain rule.

In what follows, the vectorization operation and the Kronecker product are used to avoid dealing with tensors of order larger than two. The complex conjugate of $v \in \mathbb{C}$ is denoted by $\overline{v}$, $\mathbf{0}$ denotes a matrix of zeros, $\otimes$ denotes the Kronecker product, and $\operatorname{vec} \cdot$ is the vectorization operation, which stacks the columns of a matrix to produce a column vector. Some useful relations are recalled for the convenience of the reader: (i) the absolute value squared function, $|\cdot|^2 : \mathbb{C} \to \mathbb{R}_+$ is not differentiable in the complex plane because it does not satisfy the Cauchy-Riemann equations, but is differentiable when viewed as a $\mathbb{R}^2 \to \mathbb{R}_+$ mapping, i.e., $|a + jb|^2 = a^2 + b^2$, where $a, b \in \mathbb{R}$, and its differential is given by $\mathrm{d}|a + jb|^2 = 2a\,\mathrm{d}a + 2b\,\mathrm{d}b = 2\Re\left[\overline{(a + jb)}\,\mathrm{d}(a + jb)\right]$; (ii) the differential of the matrix inverse is given by $\mathrm{d}\boldsymbol{A}^{-1} = -\boldsymbol{A}^{-1}\,\mathrm{d}\boldsymbol{A}\,\boldsymbol{A}^{-1}$; and (iii) if $\boldsymbol{X}, \boldsymbol{Y}, \boldsymbol{Z}$ are matrices such that the product $\boldsymbol{XYZ}$ is defined, then $\operatorname{vec}(\boldsymbol{XYZ}) = (\boldsymbol{Z}^\top \otimes \boldsymbol{X}) \operatorname{vec}(\boldsymbol{Y})$ —this relation is known as the "vec trick". A thorough exposition on these and other topics in matrix calculus can be found in, e.g., [57].

The sparsity pattern of these derivatives can be observed in the following block representation, derived from the functional dependency of the closed-loop transfer functions in relation to the open-loop ones, i.e., Equation (4):

$$\mathbf{D}\begin{bmatrix}\lambda_y^m\\ \lambda_u^m\\ \lambda_z^m\end{bmatrix} = \begin{bmatrix} \frac{\partial\lambda_y^m}{\partial \operatorname{vec}\boldsymbol{A}} & \frac{\partial\lambda_y^m}{\partial \operatorname{vec}\boldsymbol{B}_d} & \mathbf{0} & \frac{\partial\lambda_y^m}{\partial \operatorname{vec}\boldsymbol{C}_y} & \mathbf{0} & \frac{\partial\lambda_y^m}{\partial D_{yd}} & \mathbf{0} & \mathbf{0} & \mathbf{0} & \frac{\partial\lambda_y^m}{\partial \boldsymbol{p}} \\ \frac{\partial\lambda_u^m}{\partial \operatorname{vec}\boldsymbol{A}} & \frac{\partial\lambda_u^m}{\partial \operatorname{vec}\boldsymbol{B}_d} & \frac{\partial\lambda_u^m}{\partial \operatorname{vec}\boldsymbol{B}_u} & \frac{\partial\lambda_u^m}{\partial \operatorname{vec}\boldsymbol{C}_y} & \mathbf{0} & \frac{\partial\lambda_u^m}{\partial D_{yd}} & \frac{\partial\lambda_u^m}{\partial D_{yu}} & \mathbf{0} & \mathbf{0} & \frac{\partial\lambda_u^m}{\partial \boldsymbol{p}} \\ \frac{\partial\lambda_z^m}{\partial \operatorname{vec}\boldsymbol{A}} & \frac{\partial\lambda_z^m}{\partial \operatorname{vec}\boldsymbol{B}_d} & \frac{\partial\lambda_z^m}{\partial \operatorname{vec}\boldsymbol{B}_u} & \frac{\partial\lambda_z^m}{\partial \operatorname{vec}\boldsymbol{C}_y} & \frac{\partial\lambda_z^m}{\partial \operatorname{vec}\boldsymbol{C}_z} & \frac{\partial\lambda_z^m}{\partial D_{yd}} & \frac{\partial\lambda_z^m}{\partial D_{yu}} & \frac{\partial\lambda_z^m}{\partial D_{zd}} & \frac{\partial\lambda_z^m}{\partial D_{zu}} & \frac{\partial\lambda_z^m}{\partial \boldsymbol{p}} \end{bmatrix} \in \mathbb{R}^{3\times(n_x^2+4n_x+4+n_p)} \tag{9}$$

Expressions for each block can be obtained by evaluating the differential of the moments. Starting from the output used for feedback, y:

$$\mathrm{d}\lambda_y^m = \int_0^\infty \omega^m 2\Re\{\overline{H}_{yd}(j\omega)[\mathrm{d}S(j\omega)G_{yd}(j\omega) + S(j\omega)\,\mathrm{d}G_{yd}(j\omega)]\}\Phi_d(\omega)\,\mathrm{d}\omega \tag{10}$$

Introducing the short hand notation $\boldsymbol{\psi}_{(\cdot)}(s) = \boldsymbol{C}_{(\cdot)}(s\boldsymbol{I} - \boldsymbol{A})^{-1}$ and $\boldsymbol{\chi}_{(\cdot)} = (s\boldsymbol{I} - \boldsymbol{A})^{-1}\boldsymbol{B}_{(\cdot)}$ and expressing the differential of the open-loop transfer functions in terms of the differential of the matrices of the state space representation:

$$\begin{aligned}\mathrm{d}\lambda_y^m = \int_0^\infty \omega^m 2\Re\{\overline{H}_{yd}(j\omega)[&\frac{\partial S(j\omega)}{\partial \boldsymbol{p}}\,\mathrm{d}\boldsymbol{p}\,G_{yd}(j\omega) \\ &+ S(j\omega)(\mathrm{d}\boldsymbol{C_y}\,\boldsymbol{\chi_d}(j\omega) + \boldsymbol{\psi_y}(j\omega)\,\mathrm{d}\boldsymbol{A}\,\boldsymbol{\chi_d}(j\omega) + \boldsymbol{\psi_y}(j\omega)\,\mathrm{d}\boldsymbol{B_d} + \mathrm{d}D_{yd})]\}\Phi_d(\omega)\,\mathrm{d}\omega\end{aligned} \tag{11}$$

From inspection of Equation (11) and applying the vec-trick, the following partial derivatives may be extracted:

$$\frac{\partial\lambda_y^m}{\partial \operatorname{vec}\boldsymbol{A}} = \int_0^\infty \omega^m 2\Re\{\overline{H}_{yd}(j\omega)S(j\omega)\,\boldsymbol{\chi_d}(j\omega)^\top \otimes \boldsymbol{\psi_y}(j\omega)\}\Phi_d(\omega)\,\mathrm{d}\omega \tag{12a}$$

$$\frac{\partial\lambda_y^m}{\partial \operatorname{vec}\boldsymbol{B}_d} = \int_0^\infty \omega^m 2\Re\{\overline{H}_{yd}(j\omega)S(j\omega)\boldsymbol{\psi_y}(j\omega)\}\Phi_d(\omega)\,\mathrm{d}\omega \tag{12b}$$

$$\frac{\partial\lambda_y^m}{\partial \operatorname{vec}\boldsymbol{C}_y} = \int_0^\infty \omega^m 2\Re\{\overline{H}_{yd}(j\omega)S(j\omega)\,\boldsymbol{\chi_d}(j\omega)^\top\}\Phi_d(\omega)\,\mathrm{d}\omega \tag{12c}$$

$$\frac{\partial\lambda_y^m}{\partial D_{yd}} = \int_0^\infty \omega^m 2\Re\{\overline{H}_{yd}(j\omega)S(j\omega)\}\Phi_d(\omega)\,\mathrm{d}\omega \tag{12d}$$

$$\frac{\partial\lambda_y^m}{\partial \boldsymbol{p}} = \int_0^\infty \omega^m 2\Re\{\overline{H}_{yd}(j\omega)\frac{\partial S(j\omega)}{\partial \boldsymbol{p}}G_{yd}(j\omega)\}\Phi_d(\omega)\,\mathrm{d}\omega \tag{12e}$$

This procedure is repeated for the moments of the control input u:

$$\mathrm{d}\lambda_u^m = \int_0^\infty \omega^m 2\Re\{\overline{H}_{ud}(j\omega)G_{yu}(j\omega)^{-1}[-\mathrm{d}G_{yu}(j\omega)H_{ud}(j\omega)+\mathrm{d}S(j\omega)G_{yd}(j\omega)+(S(j\omega)-1)\,\mathrm{d}G_{yd}(j\omega)]\}\Phi_d(\omega)\,\mathrm{d}\omega \tag{13}$$

$$\mathrm{d}\lambda_u^m = \int_0^\infty \omega^m 2\Re\{\overline{H}_{yd}(j\omega)G_{yu}(j\omega)^{-1}[\\ - (\mathrm{d}\boldsymbol{C_y}\,\boldsymbol{\mathcal{X}_u}(j\omega) + \boldsymbol{\psi_y}\,\mathrm{d}\boldsymbol{A}\,\boldsymbol{\mathcal{X}_u}(j\omega) + \boldsymbol{\psi_y}(j\omega)\,\mathrm{d}\boldsymbol{B_u} + \mathrm{d}D_{yu})H_{ud}(j\omega) \\ + \frac{\partial S(j\omega)}{\partial \boldsymbol{p}}\,\mathrm{d}\boldsymbol{p}\,G_{yd}(j\omega) \\ + (S(j\omega)-1)(\mathrm{d}\boldsymbol{C_y}\,\boldsymbol{\mathcal{X}_d}(j\omega) + \boldsymbol{\psi_y}(j\omega)\,\mathrm{d}\boldsymbol{A}\,\boldsymbol{\mathcal{X}_d}(j\omega) + \boldsymbol{\psi_y}(j\omega)\,\mathrm{d}\boldsymbol{B_d} + \mathrm{d}D_{yd})]\}\Phi_d(\omega)\,\mathrm{d}\omega \quad (14)$$

From inspection of Equation (14) and applying the vec-trick, the following partial derivatives may be extracted:

$$\frac{\partial \lambda_u^m}{\partial \operatorname{vec}\boldsymbol{A}} = \int_0^\infty \omega^m 2\Re\{\overline{H}_{ud}(j\omega)G_{yu}(j\omega)^{-1}[-\boldsymbol{\mathcal{X}_u}(j\omega)^\top \otimes \boldsymbol{\psi_y}(j\omega)H_{ud}(j\omega) \\ + (S(j\omega)-1)\,\boldsymbol{\mathcal{X}_d}(j\omega)^\top \otimes \boldsymbol{\psi_y}(j\omega)]\}\Phi_d(\omega)\,\mathrm{d}\omega \quad (15a)$$

$$\frac{\partial \lambda_u^m}{\partial \operatorname{vec}\boldsymbol{B}_d} = \int_0^\infty \omega^m 2\Re\{\overline{H}_{ud}(j\omega)G_{yu}(j\omega)^{-1}(S(j\omega)-1)\boldsymbol{\psi_y}(j\omega)\}\Phi_d(\omega)\,\mathrm{d}\omega \quad (15b)$$

$$\frac{\partial \lambda_u^m}{\partial \operatorname{vec}\boldsymbol{B}_u} = -\int_0^\infty \omega^m 2\Re\{\overline{H}_{ud}(j\omega)G_{yu}(j\omega)^{-1}\boldsymbol{\psi_y}(j\omega)H_{ud}(j\omega)\}\Phi_d(\omega)\,\mathrm{d}\omega \quad (15c)$$

$$\frac{\partial \lambda_u^m}{\partial \operatorname{vec}\boldsymbol{C}_y} = \int_0^\infty \omega^m 2\Re\{\overline{H}_{ud}(j\omega)G_{yu}(j\omega)^{-1}[-\boldsymbol{\mathcal{X}_u}(j\omega)^\top H_{ud}(j\omega) + (S(j\omega)-1)\,\boldsymbol{\mathcal{X}_d}(j\omega)^\top]\}\Phi_d(\omega)\,\mathrm{d}\omega \quad (15d)$$

$$\frac{\partial \lambda_u^m}{\partial D_{yd}} = \int_0^\infty \omega^m 2\Re\{\overline{H}_{ud}(j\omega)G_{yu}(j\omega)^{-1}(S(j\omega)-1)\}\Phi_d(\omega)\,\mathrm{d}\omega \quad (15e)$$

$$\frac{\partial \lambda_u^m}{\partial D_{yu}} = -\int_0^\infty \omega^m 2\Re\{\overline{H}_{ud}(j\omega)G_{yu}(j\omega)^{-1}H_{ud}(j\omega)\}\Phi_d(\omega)\,\mathrm{d}\omega \quad (15f)$$

$$\frac{\partial \lambda_u^m}{\partial \boldsymbol{p}} = \int_0^\infty \omega^m 2\Re\{\overline{H}_{ud}(j\omega)G_{yu}(j\omega)^{-1}\frac{\partial S(j\omega)}{\partial \boldsymbol{p}}G_{yd}(j\omega)\}\Phi_d(\omega)\,\mathrm{d}\omega \quad (15g)$$

And finally the procedure is repeated for the moments of the output not used for feedback z:

$$\mathrm{d}\lambda_z^m = \int_0^\infty \omega^m 2\Re\Big\{\overline{H}_{zd}(j\omega)\Big[\mathrm{d}\boldsymbol{C_z}\,\boldsymbol{\mathcal{X}_d}(j\omega) + \boldsymbol{\psi_z}(j\omega)\,\mathrm{d}\boldsymbol{A}\,\boldsymbol{\mathcal{X}_d}(j\omega) + \boldsymbol{\psi_z}(j\omega)\,\mathrm{d}\boldsymbol{B_d} + \mathrm{d}D_{zd} \\ (\mathrm{d}\boldsymbol{C_z}\,\boldsymbol{\mathcal{X}_u}(j\omega) + \boldsymbol{\psi_z}(j\omega)\,\mathrm{d}\boldsymbol{A}\,\boldsymbol{\mathcal{X}_u}(j\omega) + \boldsymbol{\psi_z}(j\omega)\,\mathrm{d}\boldsymbol{B_u} + \mathrm{d}D_{zu})H_{ud}(j\omega) \\ + G_{yu}(j\omega)^{-1}\Big(-(\mathrm{d}\boldsymbol{C_y}\,\boldsymbol{\mathcal{X}_u}(j\omega) + \boldsymbol{\psi_y}\,\mathrm{d}\boldsymbol{A}\,\boldsymbol{\mathcal{X}_u}(j\omega) + \boldsymbol{\psi_y}(j\omega)\,\mathrm{d}\boldsymbol{B_u} + \mathrm{d}D_{yu})H_{ud}(j\omega) \\ + \frac{\partial S(j\omega)}{\partial \boldsymbol{p}}\,\mathrm{d}\boldsymbol{p}\,G_{yd}(j\omega) \\ + (S(j\omega)-1)(\mathrm{d}\boldsymbol{C_y}\,\boldsymbol{\mathcal{X}_d}(j\omega) + \boldsymbol{\psi_y}(j\omega)\,\mathrm{d}\boldsymbol{A}\,\boldsymbol{\mathcal{X}_d}(j\omega) + \boldsymbol{\psi_y}(j\omega)\,\mathrm{d}\boldsymbol{B_d} + \mathrm{d}D_{yd})\Big)\Big]\Big\}\Phi_d(\omega)\,\mathrm{d}\omega \quad (16)$$

From inspection of Equation (16) and applying the vec-trick, the following partial derivatives may be extracted:

$$\frac{\partial \lambda_z^m}{\partial \operatorname{vec} \boldsymbol{A}} = \int_0^\infty \omega^m 2\Re\{\overline{H}_{zd}(j\omega)[\,\boldsymbol{\chi_d}(j\omega)^\top \otimes \boldsymbol{\psi_z}(j\omega) + \boldsymbol{\chi_u}(j\omega)^\top \otimes \boldsymbol{\psi_z}(j\omega) H_{ud}(j\omega) + G_{zu}(j\omega)(-G_{yu}(j\omega)^{-1}\boldsymbol{\chi_u}(j\omega)^\top \otimes \boldsymbol{\psi_y}(j\omega) H_{ud}(j\omega) + G_{yu}(j\omega)^{-1}(S(j\omega)-1)\,\boldsymbol{\chi_d}(j\omega)^\top \otimes \boldsymbol{\psi_y}(j\omega))]\}\Phi_d(\omega)\,\mathrm{d}\omega \tag{17a}$$

$$\frac{\partial \lambda_z^m}{\partial \operatorname{vec} \boldsymbol{B}_d} = \int_0^\infty \omega^m 2\Re\{\overline{H}_{zd}(j\omega)[\boldsymbol{\psi_z}(j\omega) + G_{zu}(j\omega)G_{yu}(j\omega)^{-1}(S(j\omega)-1)\boldsymbol{\psi_y}(j\omega)]\}\Phi_d(\omega)\,\mathrm{d}\omega \tag{17b}$$

$$\frac{\partial \lambda_z^m}{\partial \operatorname{vec} \boldsymbol{B}_u} = \int_0^\infty \omega^m 2\Re\{\overline{H}_{zd}(j\omega)[\boldsymbol{\psi_z}(j\omega) - G_{zu}(j\omega)G_{yu}(j\omega)^{-1}\boldsymbol{\psi_y}(j\omega)]H_{ud}(j\omega))]\}\Phi_d(\omega)\,\mathrm{d}\omega \tag{17c}$$

$$\frac{\partial \lambda_z^m}{\partial \operatorname{vec} \boldsymbol{C}_y} = \int_0^\infty \omega^m 2\Re\{\overline{H}_{zd}(j\omega)G_{zu}(j\omega)G_{yu}(j\omega)^{-1}[-\boldsymbol{\chi_u}(j\omega)^\top H_{ud}(j\omega) + (S(j\omega)-1)\,\boldsymbol{\chi_d}(j\omega)^\top]\}\Phi_d(\omega)\,\mathrm{d}\omega \tag{17d}$$

$$\frac{\partial \lambda_z^m}{\partial \operatorname{vec} \boldsymbol{C}_z} = \int_0^\infty \omega^m 2\Re\{\overline{H}_{zd}(j\omega)[\,\boldsymbol{\chi_d}(j\omega)^\top + \boldsymbol{\chi_u}(j\omega)^\top H_{ud}(j\omega))]\}\Phi_d(\omega)\,\mathrm{d}\omega \tag{17e}$$

$$\frac{\partial \lambda_z^m}{\partial D_{yd}} = \int_0^\infty \omega^m 2\Re\{\overline{H}_{zd}(j\omega)G_{zu}(j\omega)G_{yu}(j\omega)^{-1}(S(j\omega)-1)\}\Phi_d(\omega)\,\mathrm{d}\omega \tag{17f}$$

(17g)

$$\frac{\partial \lambda_z^m}{\partial D_{yu}} = -\int_0^\infty \omega^m 2\Re\{\overline{H}_{zd}(j\omega)G_{zu}(j\omega)G_{yu}(j\omega)^{-1}H_{ud}(j\omega)\}\Phi_d(\omega)\,\mathrm{d}\omega \tag{17h}$$

$$\frac{\partial \lambda_z^m}{\partial D_{zd}} = \int_0^\infty \omega^m 2\Re\{\overline{H}_{zd}(j\omega)\}\Phi_d(\omega)\,\mathrm{d}\omega \tag{17i}$$

$$\frac{\partial \lambda_z^m}{\partial D_{zu}} = \int_0^\infty \omega^m 2\Re\{\overline{H}_{zd}(j\omega)H_{ud}(j\omega)\}\Phi_d(\omega)\,\mathrm{d}\omega \tag{17j}$$

$$\frac{\partial \lambda_z^m}{\partial \boldsymbol{p}} = \int_0^\infty \omega^m 2\Re\{\overline{H}_{ud}(j\omega)G_{zu}(j\omega)G_{yu}(j\omega)^{-1}\frac{\partial S(j\omega)}{\partial \boldsymbol{p}}G_{yd}(j\omega)\}\Phi_d(\omega)\,\mathrm{d}\omega \tag{17k}$$

III. Application to the Evaluation of Turbulence Rejection During Landing

A. Aircraft model

The proposed metrics are used to analyze a longitudinal model of a rigid aircraft with steady aerodynamics in the approach-to-landing condition. The choice of a rigid model is based on previous studies that showed that flexibility effects do not greatly impact the global behavior of the Supersonic Configuration at Low Speeds (SCALOS) aircraft [58]. The aerodynamic coefficients are obtained from the parameterized surrogate model of the SCALOS aircraft described in [55]. A schematic drawing of the aircraft along with a description of the available design variables is shown in Figure 2. This section presents both the nonlinear and linearized models employed. The nonlinear model is used for trim, while the linearized model around the trimmed condition is used to compute the metrics. The inputs to the models are vertical gust velocity, w, and elevator deflection, η, while the outputs are the displacement normal to the approach ramp, ΔGL (which depends on the approach ramp angle γ_R) and the angle of attack, α. The states are the velocity components in the body axis, U and W, pointing forward and down respectively, the pitch rate Q and the pitch attitude θ. The notation used was based on [59].

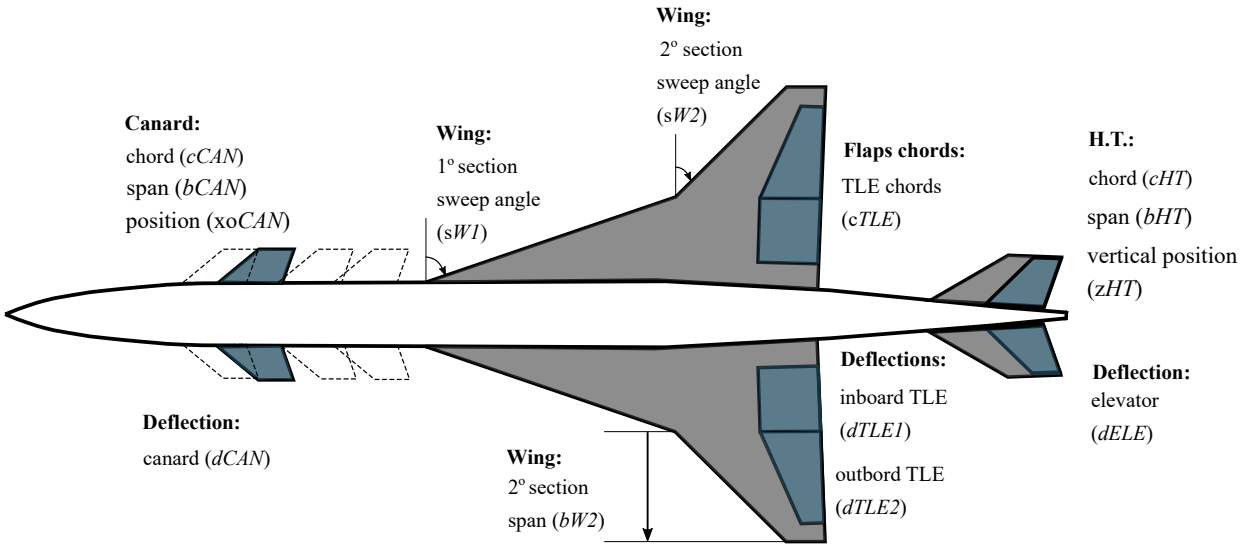

Fig. 2 SCALOS UW-S-15W configuration with the parameterization variables highlighted (reprinted from [55], with permission)

1. Nonlinear model

The nonlinear model is given by the following system of ordinary differential equations (ODEs):

$$\dot{U} = -QW - g\sin\theta + (X+T)/m \tag{18a}$$

$$\dot{W} = QU + g\cos\theta + Z/m \tag{18b}$$

$$\dot{Q} = M/J \tag{18c}$$

$$\dot{\theta} = Q \tag{18d}$$

$$\tfrac{\mathrm{d}}{\mathrm{d}t}\Delta\mathrm{GL} = V^{\mathrm{GL}} = U\sin(\theta-\gamma_R) - W\cos(\theta-\gamma_R) \tag{18e}$$

where g is the acceleration of gravity; X and Z are the aerodynamic forces pointing forward and down, respectively; m is the mass of the aircraft; M is the aerodynamic pitch-up moment; J is the aircraft's moment of inertia; and V^{GL} is the velocity component normal to the approach ramp.

This ODE system is linked to the surrogate aerodynamic model via the auxiliary equations:

$$\alpha = \tan^{-1}\left(\frac{W - w\cos(\theta)}{U + w\sin(\theta)}\right) \tag{19a}$$

$$\bar{q} = \tfrac{1}{2}\rho\left((U + w\sin(\theta))^2 + (W - w\cos(\theta))^2\right) \tag{19b}$$

$$X = \sin(\alpha)\,\bar{q}SC_L(\alpha, Q, \eta) - \cos(\alpha)\,\bar{q}SC_D(\alpha, \eta) \tag{19c}$$

$$Z = -\cos(\alpha)\,\bar{q}SC_L(\alpha, Q, \eta) - \sin(\alpha)\,\bar{q}SC_D(\alpha, \eta) \tag{19d}$$

$$M = \bar{q}ScC_M(\alpha, Q, \eta) \tag{19e}$$

where $\bar{q}$ is the dynamic pressure; ρ is the air density; S is the wing reference area; c is the mean aerodynamic chord; and C_L, C_D and C_M are the aerodynamic coefficients of lift, drag, and moment respectively.

2. Linearized model

The nonlinear equations of motion derived for the body-axis frame and presented in the previous section can be linearized for any particular equilibrium point (trim point), to yield a state space representation in the form of (1), where $\boldsymbol{x} = [U \quad W \quad Q \quad \theta \quad \Delta\mathrm{GL}]^\intercal$ is the state vector, $d = w$ is the disturbance, $u = \eta$ is the control input, $y = \Delta\mathrm{GL}$ is the

output used for feedback, and $z = \alpha$ is the output not used for feedback. The state space's matrices are given by

$$\left[\begin{array}{c|c} \boldsymbol{A} & \boldsymbol{B} \\ \hline \boldsymbol{C} & \boldsymbol{D} \end{array}\right] = \left[\begin{array}{c|cc} \boldsymbol{A} & \boldsymbol{B}_d & \boldsymbol{B}_u \\ \hline \boldsymbol{C}_y & D_{yd} & D_{yu} \\ \boldsymbol{C}_z & D_{zd} & D_{zu} \end{array}\right] = \left[\begin{array}{ccccc|cc} X_U & X_W & X_Q - W_{\text{trim}} & -g\cos\theta_{\text{trim}} & 0 & X_w & X_\eta \\ Z_U & Z_W & Z_Q + U_{\text{trim}} & -g\sin\theta_{\text{trim}} & 0 & Z_w & Z_\eta \\ M_U & M_W & M_Q & 0 & 0 & M_w & M_\eta \\ 0 & 0 & 1 & 0 & 0 & 0 & 0 \\ V_U^{\text{GL}} & V_W^{\text{GL}} & 0 & V_\theta^{\text{GL}} & 0 & 0 & 0 \\ \hline 0 & 0 & 0 & 0 & 1 & 0 & 0 \\ \alpha_U & \alpha_W & 0 & 0 & 0 & \alpha_w & 0 \end{array}\right] \tag{20}$$

The elements of these matrices include the dimensional derivatives defined in Table 1, which, in turn, are functions of the model parameters, the trim condition (denoted by variables with the subscript "trim"), the aerodynamic coefficients, and the aerodynamic derivatives. The terms related to $C_{D\,\alpha}$ and $C_{D\,\eta}$ are neglected since their inclusion does not substantially change the dynamics of the system.

B. Integration limits

Due to the presence of the non-zero passthrough term D_{zd}, the output z will not have a finite second moment. However, the existence of this term is due to modeling simplifications such as not considering the unsteady aerodynamic effects, especially the roll-off of the gust-to-outputs transfer functions when the gust spacial frequency gets close to the dimensions of the wing of the aircraft (i.e., the "averaging of gust velocity" over chord and span), the faster decrease of the PSD in the "viscous subrange", and the effect of flexibility in the aircraft structure at high frequencies. These simplifications are discussed in [10, Appendix E]. Due to these modeling inaccuracies at high frequencies, the integration of the PSDs to obtain the spectral moments of the signals of interest is not carried out to infinity, but rather to the frequency of 20 Hz. Replacing the surrogate aerodynamic model of [55] by linearized unsteady vortex lattice method (UVLM) aerodynamics enhanced with vortex lift, such as the one described in [60] will help to eliminate some of these simplifications and is left as future work.

C. Sensitivity function parameterization

In order to design the sensitivity function, it must be parameterized. For this work, the sensitivity function is parameterized by considering a series arrangement of a second-order Butterworth high-pass filter and one peaking filter, i.e.,

$$S(s) = \underbrace{\frac{s^2}{s^2 + \sqrt{2}\omega_c s + \omega_c^2}}_{\text{high-pass filter}} \underbrace{\frac{s^2 + g_0\omega_0/q_0 + {\omega_0}^2}{s^2 + \omega_0/q_0 + {\omega_0}^2}}_{\text{peaking filter}} \tag{21}$$

The parameters of the sensitivity function are the high-pass filter's cutoff frequency ω_c, and the peaking filter's gain g_0, center frequency ω_0, and quality factor q_0.

The peak of the magnitude of the sensitivity function is related to the robustness of the closed-loop system, specifically, the sensitivity peak magnitude M_S is the minimum distance between the Nyquist curve and the critical point $(-1 + j0)$ [61]. The following bounds on gain and phase margins can be stated in terms of M_S:

$$\text{GM} \geq \frac{M_S}{M_S - 1} \qquad\qquad \text{PM} \geq 2\sin^{-1}\left(\frac{1}{2M_S}\right) \tag{22}$$

For example, $M_S \leq 2$ guarantees a gain margin of at least 6 dB and phase margin of at least 29 deg, which are usual requirements for control design. For this parameterization, it is easy to see that $M_S \leq g_0$, therefore robustness of the design can be guaranteed via a bound on g_0.

The sensitivity function must satisfy the Bode integral relation [44, 45], a fundamental limitation of control:

$$\int_0^\infty \log|S(j\omega)|\mathrm{d}\omega = \pi \sum_{k=0}^{n_u} \Re(p_k^+) \tag{23}$$

where p_k^+, $i = 1, 2, \ldots, n_u$, denotes the open right half plane poles of the open-loop system.

Table 1 Dimensional derivatives for linearized longitudinal rigid aircraft model

A matrix

$$X_U = \frac{1}{m} S\rho \left(\left(-C_D U_{\text{trim}} - \tfrac{1}{2} W_{\text{trim}} C_{L\text{trim}} \right) \cos(\alpha_{\text{trim}}) + \left(-\tfrac{1}{2} C_D W_{\text{trim}} + U_{\text{trim}} C_{L\text{trim}} - \tfrac{1}{2} W_{\text{trim}} C_{L\alpha} \right) \sin(\alpha_{\text{trim}}) \right)$$

$$X_W = \frac{1}{m} S\rho \left(\left(-C_D W_{\text{trim}} + \tfrac{1}{2} U_{\text{trim}} C_{L\text{trim}} \right) \cos(\alpha_{\text{trim}}) + \left(\tfrac{1}{2} C_D U_{\text{trim}} + \tfrac{1}{2} U_{\text{trim}} C_{L\alpha} + W_{\text{trim}} C_{L\text{trim}} \right) \sin(\alpha_{\text{trim}}) \right)$$

$$X_Q = \frac{1}{m} \bar{q}_{\text{trim}} S C_{LQ} \sin(\alpha_{\text{trim}})$$

$$Z_U = \frac{1}{m} S\rho \left(\left(-C_D U_{\text{trim}} - \tfrac{1}{2} W_{\text{trim}} C_{L\text{trim}} \right) \sin(\alpha_{\text{trim}}) + \left(\tfrac{1}{2} C_D W_{\text{trim}} - U_{\text{trim}} C_{L\text{trim}} + \tfrac{1}{2} W_{\text{trim}} C_{L\alpha} \right) \cos(\alpha_{\text{trim}}) \right)$$

$$Z_W = \frac{1}{m} S\rho \left(\left(-C_D W_{\text{trim}} + \tfrac{1}{2} U_{\text{trim}} C_{L\text{trim}} \right) \sin(\alpha_{\text{trim}}) + \left(-\tfrac{1}{2} C_D U_{\text{trim}} - \tfrac{1}{2} U_{\text{trim}} C_{L\alpha} - W_{\text{trim}} C_{L\text{trim}} \right) \cos(\alpha_{\text{trim}}) \right)$$

$$Z_Q = -\frac{1}{m} \bar{q}_{\text{trim}} S C_{LQ} \cos(\alpha_{\text{trim}})$$

$$M_U = -\frac{1}{2J} Sc\rho W_{\text{trim}} C_{M\alpha}$$

$$M_W = \frac{1}{2J} Sc\rho U_{\text{trim}} C_{M\alpha}$$

$$M_Q = \frac{1}{J} \bar{q}_{\text{trim}} Sc C_{MQ}$$

$$V_U^{GL} = \sin(\theta_{\text{trim}} - \gamma_R)$$

$$V_W^{GL} = -\cos(\theta_{\text{trim}} - \gamma_R)$$

$$V_\theta^{GL} = U_{\text{trim}} \cos(\theta_{\text{trim}} - \gamma_R) + W_{\text{trim}} \sin(\theta_{\text{trim}} - \gamma_R)$$

B matrix

$$\begin{aligned} X_w = \frac{1}{m} S\rho (& -\tfrac{1}{2} C_{L\text{trim}} \left(U_{\text{trim}} \cos(\theta_{\text{trim}}) + W_{\text{trim}} \sin(\theta_{\text{trim}}) \right) \cos(\alpha_{\text{trim}}) \\ & + \left(-\tfrac{1}{2} C_D \left(U_{\text{trim}} \cos(\theta_{\text{trim}}) + W_{\text{trim}} \sin(\theta_{\text{trim}}) \right) - \tfrac{1}{2} C_{L\alpha} \left(U_{\text{trim}} \cos(\theta_{\text{trim}}) + W_{\text{trim}} \sin(\theta_{\text{trim}}) \right) \right) \sin(\alpha_{\text{trim}}) \\ & + \left(-C_D \cos(\alpha_{\text{trim}}) + C_{L\text{trim}} \sin(\alpha_{\text{trim}}) \right) \left(U_{\text{trim}} \sin(\theta_{\text{trim}}) - W_{\text{trim}} \cos(\theta_{\text{trim}}) \right)) \end{aligned}$$

$$\begin{aligned} Z_w = \frac{1}{m} S\rho (& -\tfrac{1}{2} C_{L\text{trim}} \left(U_{\text{trim}} \cos(\theta_{\text{trim}}) + W_{\text{trim}} \sin(\theta_{\text{trim}}) \right) \sin(\alpha_{\text{trim}}) \\ & + \left(\tfrac{1}{2} C_D \left(U_{\text{trim}} \cos(\theta_{\text{trim}}) + W_{\text{trim}} \sin(\theta_{\text{trim}}) \right) + \tfrac{1}{2} C_{L\alpha} \left(U_{\text{trim}} \cos(\theta_{\text{trim}}) + W_{\text{trim}} \sin(\theta_{\text{trim}}) \right) \right) \cos(\alpha_{\text{trim}}) \\ & - \left(C_D \sin(\alpha_{\text{trim}}) + C_{L\text{trim}} \cos(\alpha_{\text{trim}}) \right) \left(U_{\text{trim}} \sin(\theta_{\text{trim}}) - W_{\text{trim}} \cos(\theta_{\text{trim}}) \right)) \end{aligned}$$

$$M_w = \frac{1}{J} Sc\rho \left(-\tfrac{1}{2} C_{M\alpha} \left(U_{\text{trim}} \cos(\theta_{\text{trim}}) + W_{\text{trim}} \sin(\theta_{\text{trim}}) \right) - W_{\text{trim}} \cos(\theta_{\text{trim}}) \right)$$

$$Z_\eta = -\frac{1}{m} \bar{q}_{\text{trim}} S C_{L\eta} \cos(\alpha_{\text{trim}})$$

$$X_\eta = \frac{1}{m} \bar{q}_{\text{trim}} S C_{L\eta} \sin(\alpha_{\text{trim}})$$

$$M_\eta = \frac{1}{J} \bar{q}_{\text{trim}} Sc C_{M\eta}$$

C matrix

$$\alpha_U = -\frac{W_{\text{trim}}}{U_{\text{trim}}^2 + W_{\text{trim}}^2}$$

$$\alpha_W = \frac{U_{\text{trim}}}{U_{\text{trim}}^2 + W_{\text{trim}}^2}$$

D matrix

$$\alpha_w = -\frac{U_{\text{trim}} \cos(\theta_{\text{trim}}) + W_{\text{trim}} \sin(\theta_{\text{trim}})}{U_{\text{trim}}^2 + W_{\text{trim}}^2}$$

D. Sensitivity function design

A simplified optimization problem is considered for computing the parameters of the sensitivity function. It consists of minimizing the sum of the probabilities of the signals of interest exceeding pre-established limits while enforcing a limit on g_0 for the robustness, as discussed in the previous section, and a constraint on the Bode integral relation. It can be stated as:

$$
\begin{aligned}
\text{minimize} \quad & \mathbb{P}(\{\Delta\text{GL} < -10\,\text{m}\} \cup \{\Delta\text{GL} > 10\,\text{m}\}) \\
& + \mathbb{P}(\{\alpha < -10\,\text{deg}\} \cup \{\alpha > 40\,\text{deg}\}) \\
& + \mathbb{P}(\{\eta < -30\,\text{deg}\} \cup \{\eta > 30\,\text{deg}\}) \\
& + \mathbb{P}(\{\dot{\eta} < -60\,\text{deg/s}\} \cup \{\dot{\eta} > 60\,\text{deg/s}\}) \\
\text{with respect to} \quad & \omega_c, \omega_0, g_0, q_0 \\
\text{such that} \quad & g_0 \leq 2 \\
& \int_0^\infty \log |S(j\omega)| \, \mathrm{d}\omega = \pi \sum_{k=0}^{n_u} \Re(p_k^+)
\end{aligned}
$$

where the sensitivity function is parameterized as proposed in Equation (21).

IV. Results

A. Trim condition and poles of the linearized system

The Equations of the nonlinear model (18) were solved using NASA OpenMDAO's Newton solver [62] in order to find a equilibrium condition for flying an approach ramp of −3 deg with a 20 deg angle of attack. The equilibrium states along with related quantities are:

$U_{\text{trim}} = 93\,\text{m/s}$	$W_{\text{trim}} = 34\,\text{m/s}$	$T_{\text{trim}} = 25\,\text{kN}$
$\theta_{\text{trim}} = 17\,\text{deg}$	$\alpha_{\text{trim}} = 20\,\text{deg}$	$\eta_{\text{trim}} = -19\,\text{deg}$
$C_{D\text{trim}} = 0.21$	$C_{L\text{trim}} = 0.63$	
$C_{L\alpha\text{trim}} = 1.58$	$C_{L\eta\text{trim}} = 0.07$	$C_{LQ\text{trim}} = -0.03$
$C_{M\alpha\text{trim}} = -0.02$	$C_{M\eta\text{trim}} = -0.15$	$C_{MQ\text{trim}} = -0.02$

The dynamical system was linearized around this point using Equation (20) and Table 1, which resulted in a open-loop system with the following poles:

$$
\begin{aligned}
p_1 &= 0.00\,\text{rad/s} \\
p_2 &= (-0.19 + j0.40)\,\text{rad/s} \\
p_3 &= (-0.19 - j0.40)\,\text{rad/s} \\
p_4 &= (-0.02 + j0.12)\,\text{rad/s} \\
p_5 &= (-0.02 - j0.12)\,\text{rad/s}
\end{aligned}
$$

The first pole is a pure integrator and is related to the integration of the velocity of glideslope deviation into the glideslope deviation itself, the first conjugate pair corresponds to the short-period mode, and the second pair is related to the phugoid mode. Figure 3a shows the Bode plots for the open-loop linearized system.

B. Turbulence rejection metrics

The optimization problem for sensitivity function design shown in Section III.D was solved using SciPy's SLSQP optimizer [63] to a tolerance of 10^{-8}, which converged in 18 iterations. The optimal values for the sensitivity function parameters were $\omega_c = 0.94\,\text{rad/s}, \omega_0 = 1.05\,\text{rad/s}, g_0 = 1.88, q_0 = 0.71$. The calculated turbulence rejection metrics for the trim condition described in the previous section and the optimized sensitivity function defined are shown in Table 2, along with relevant statistical parameters and the design limits for each quantity of interest. The von Kármán turbulence disturbance considered in the calculations had an intensity of 10 ft/s and a characteristic scale of 2500 ft.

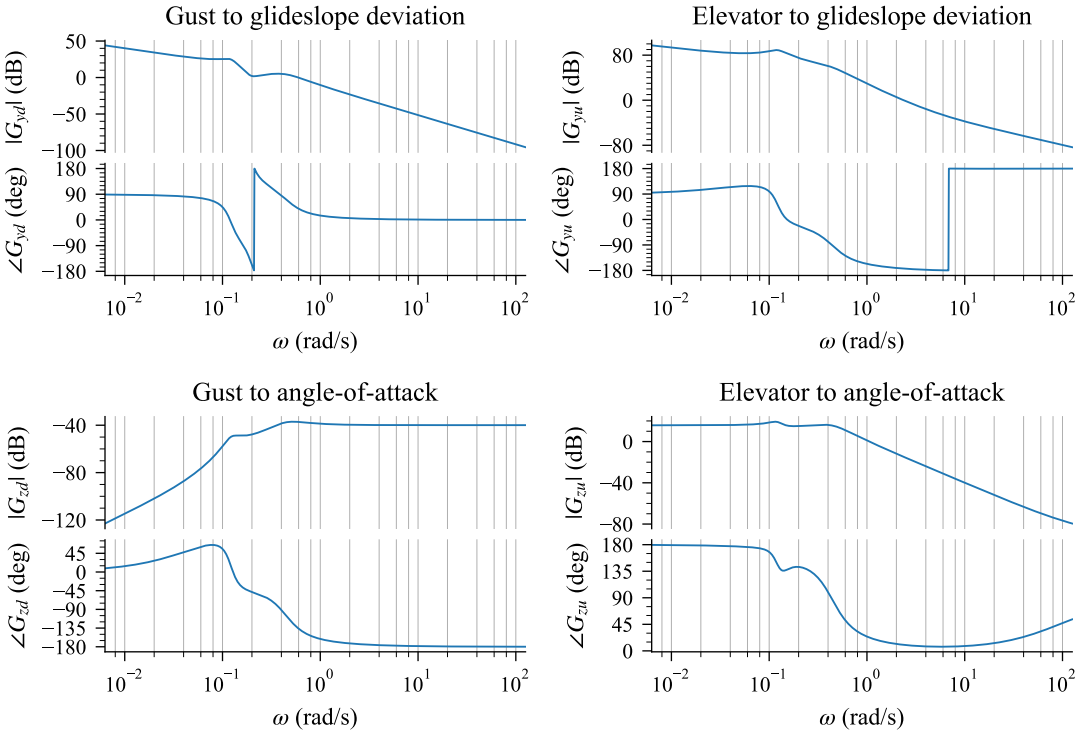

(a) open-loop

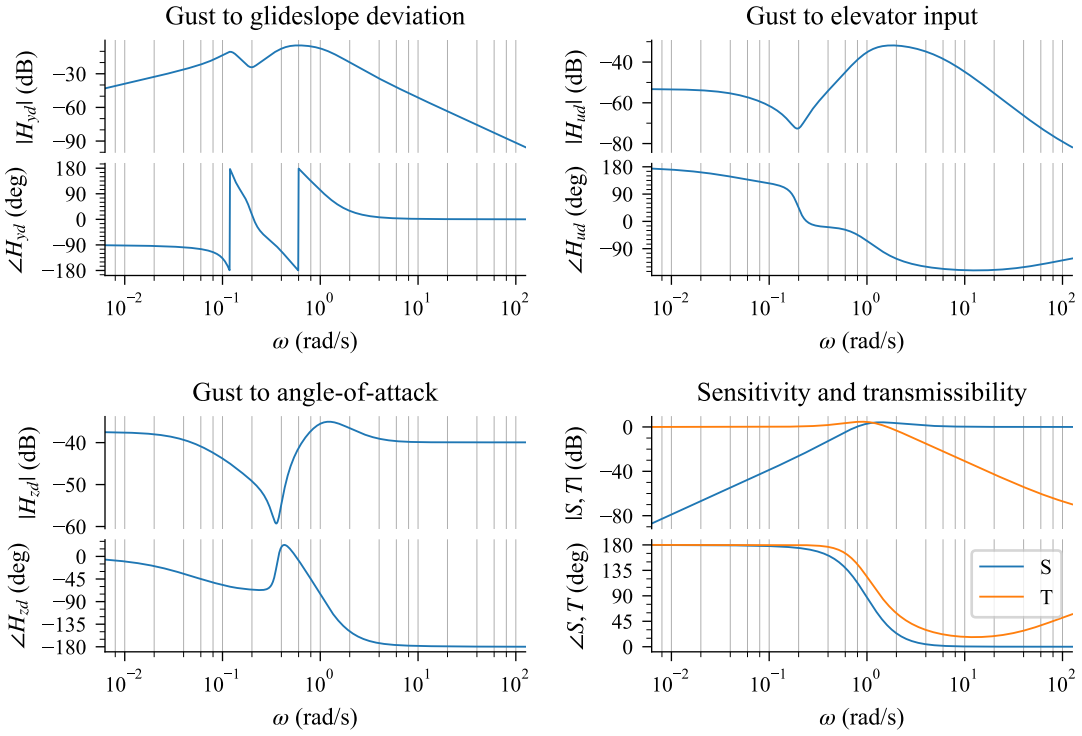

(b) closed-loop

Fig. 3 Bode plots for longitudinal aircraft model.

Table 2 Design metrics, design limits, mean and standard deviation for the quantities of interest

	Probability of exceedance (-)	Frequency of Exceedance (1/s)	Frequency of mean crossings (1/s)	Lower limit	Upper limit	Mean	Standard deviation	Units
Glideslope deviation	0.04	0.05	0.20	−10.00	10.00	0.00	4.82	(m)
Angle of attack	0.04	0.54	2.22	−10.00	40.00	20.00	11.27	(deg)
Elevator deflection	0.12	0.28	0.78	−30.00	30.00	−19.48	8.92	(deg)
Elevator rate	0.01	0.26	2.40	−60.00	60.00	0.00	21.93	(deg/s)

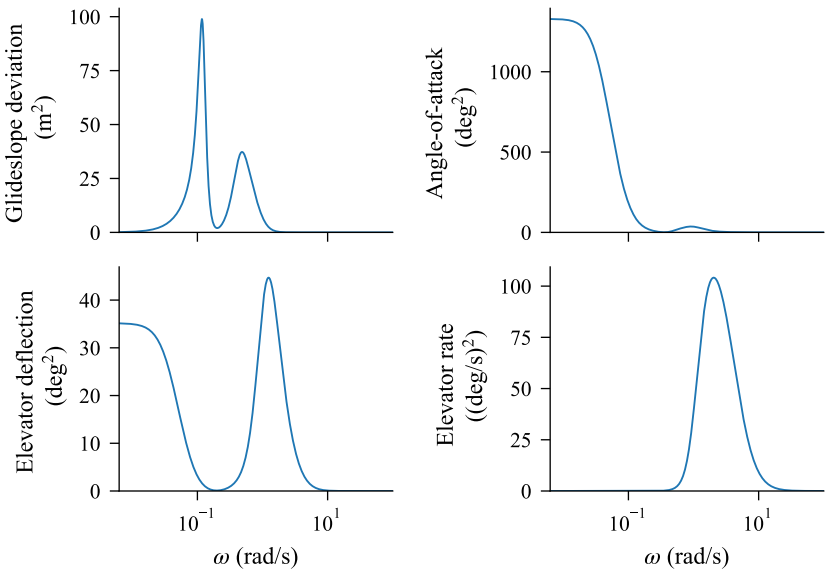

Fig. 4 Power spectral densities for the quantities of interest.

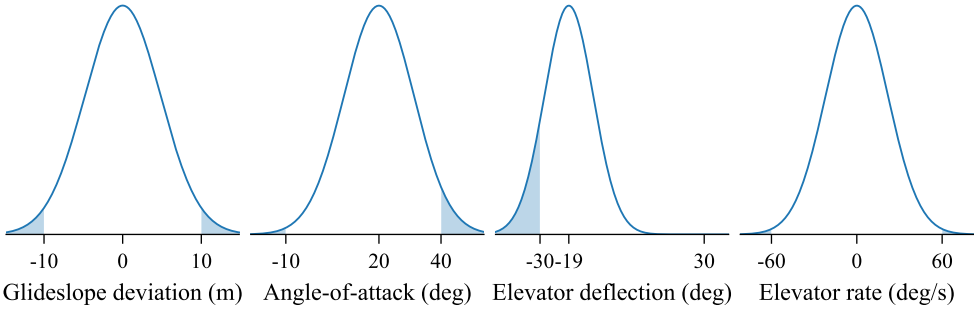

Fig. 5 Probability density functions for the quantities of interest. The portion outside the design limits is highlighted, and the values shown correspond to the lower limit, trim value, and upper limit.

The optimal design has low bandwidth if compared to the available bandwidth for this class of airplanes (usually well over 10 Hz. This is due to the elevator deflection needed for trimming the aircraft (-19.5 deg) being relatively close to the lower limit of -30 deg. Indeed, the probability of exceeding the elevator deflection limits (12%) is the higher of the probabilities being minimized, followed by the probability of exceeding angle of attack or glideslope deviation limits (both at 4%) and the probability of exceeding the elevator rate limit (1%). The low bandwidth of the control loop reduces the control action but at the cost of poor regulation. These metrics indicate that this design does not have good turbulence rejection performance.

More insight into the calculated metrics can be obtained from analyzing the closed-loop Bode plots in Figure 3b, the probability density functions (PDF) in Figure 5, and the power spectral densities in Figure 4. The chosen parameterization for the sensitivity function adds two (closed-loop) zeros at the origin of the gust to glideslope deviation transfer function, one that cancels the integrator from the deviation velocity and another one that removes the steady state error, as can be seen in its PSD, which is zero at zero frequency and has peaks at the phugoid and short-period modes. The angle of attack PSD shows very high spectral content in low frequencies, and another peak for the short-period mode, which contributes to the relatively high expected frequency of exceedance and mean-crossings for this quantity.

C. Derivative verification

The analytical derivatives presented in Section II.B were verified against a finite differences approximation at the analysis point described in Section IV.A. The finite difference approximation was done using a central difference scheme and step size equal to 10^{-8} times the element being perturbed, but not smaller than an absolute step size of 10^{-8}. The analytical and finite differences derivatives were in the very good agreement, as shown in Table 3 for the zeroeth order moment. The relative error between the methods was calculated as

$$\text{Relative error} = \frac{\|\text{FD derivatives} - \text{Analytical derivatives}\|}{\|\text{Analytical derivatives}\|} \tag{25}$$

where $\|\cdot\|$ denotes the Euclidean norm. The maximum relative error of the comparison was of 1.29×10^{-8}.

D. Sensitivity analysis

More insight into the configuration being analyzed can be gathered from the derivatives shown in Table 4. It is seen that moving the CG aft will improve every metric, possibly due to reducing the static elevator deflection necessary to trim the aircraft, as well as making it more responsive to control input (less stable). However, if the aircraft becomes open-loop unstable, the right-hand side of the Bode integral relation (23) will be greater than zero, which will penalize performance. This effect cannot be captured by a derivative analysis of a stable design due to the derivative discontinuity in the Bode integral relation when a pole crosses the imaginary axis. Increasing wing area will benefit most metrics but penalize elevator deflection. Increasing the chord and span of the canard will reduce the exceedance events of elevator deflection, likely because it also has a destabilizing effect. Increasing the horizontal tail dimensions will help with that as well, this time because of increased control effectiveness. Introducing static deflections in the wing's trailing edge flaps or in the canard has small effects on the metrics because they are not very effective for trimming the vehicle. It

Table 3 Verification of the analytic derivatives against finite differences.

of	w.r.t.	Euclidean norm	Relative error
λ_y^0	vec $\boldsymbol{A}$	$8.04 \times 10^{+4}$	1.29×10^{-8}
	vec $\boldsymbol{B}$	$1.06 \times 10^{+4}$	3.75×10^{-11}
	vec $\boldsymbol{C}$	$5.12 \times 10^{+1}$	4.49×10^{-9}
	vec $\boldsymbol{D}$	$4.52 \times 10^{+1}$	4.60×10^{-9}
λ_z^0	vec $\boldsymbol{A}$	$5.31 \times 10^{+1}$	4.66×10^{-10}
	vec $\boldsymbol{B}$	$2.55 \times 10^{+1}$	3.22×10^{-11}
	vec $\boldsymbol{C}$	$1.27 \times 10^{+1}$	4.84×10^{-11}
	vec $\boldsymbol{D}$	3.36	9.72×10^{-11}
λ_u^0	vec $\boldsymbol{A}$	$1.53 \times 10^{+1}$	7.02×10^{-11}
	vec $\boldsymbol{B}$	$1.68 \times 10^{+1}$	3.77×10^{-11}
	vec $\boldsymbol{C}$	6.70×10^{-1}	6.55×10^{-10}
	vec $\boldsymbol{D}$	1.08	7.66×10^{-11}

Table 4 Selected design derivatives, color mapped by value.

(a) with respect to geometric parameters

	CG position	bW2	bCAN	cCAN	bHT	cHT	dTLE1	dTLE2	dCAN
$\mathbb{P}$, ΔGL	−0.038	−0.024	0.004	0.002	0.001	0.000	−0.001	−0.001	0.000
$\mathbb{P}$, α	−0.020	−0.012	0.002	0.001	0.000	0.000	0.000	0.000	0.000
$\mathbb{P}$, η	−5.628	0.503	−0.221	−0.023	−0.171	−0.081	0.019	0.021	−0.004
$\mathbb{P}$, $\dot{\eta}$	−0.011	−0.007	0.001	0.001	0.000	0.000	0.000	0.000	0.000
$\mathbb{E}[N]$, ΔGL	−0.021	−0.013	0.002	0.001	0.000	0.000	0.000	0.000	0.000
$\mathbb{E}[N]$, α	−0.166	−0.103	0.018	0.008	0.004	0.000	−0.003	−0.002	0.000
$\mathbb{E}[N]$, η	−4.604	0.411	−0.180	−0.019	−0.139	−0.066	0.016	0.017	−0.003
$\mathbb{E}[N]$, $\dot{\eta}$	−0.211	−0.131	0.023	0.010	0.005	0.000	−0.003	−0.003	0.000

(b) with respect to sensitivity function parameters

	ω_c	ω_0	g_0	q_0
$\mathbb{P}$, ΔGL	−0.341	−0.052	0.063	−0.046
$\mathbb{P}$, α	−0.045	0.005	0.027	−0.011
$\mathbb{P}$, η	0.142	0.169	0.092	−0.136
$\mathbb{P}$, $\dot{\eta}$	0.058	0.039	0.010	−0.042
$\mathbb{E}[N]$, ΔGL	−0.156	−0.023	0.040	−0.023
$\mathbb{E}[N]$, α	−0.114	0.014	0.071	−0.032
$\mathbb{E}[N]$, η	0.259	0.149	0.018	−0.177
$\mathbb{E}[N]$, $\dot{\eta}$	2.667	−0.667	−1.484	1.208

is worth noting that changes in the geometric variables at this design point will affect the metrics related to elevator deflection most strongly.

We now turn our attention to the variables parameterizing the sensitivity function, starting with their effects on the probability of exceedance of design limits for the various signals of interest. Increasing ω_c is beneficial for the metrics related to the outputs (angle of attack and glideslope deviation) because it increases the bandwidth of the control loop but is detrimental to the metrics related to the control input (η) and control input rate ($\dot{\eta}$). Increasing ω_0 is only beneficial to the variable being used for feedback, i.e., glideslope deviation. Increasing g_0 or decreasing q_0, that is, making the peak in the sensitivity higher or wider is detrimental for all probability metrics. These comments also hold for the expected frequency of exceedance metrics, except for the ones relative to the rate of elevator deflection. This unexpected behavior requires further investigation in order to be properly understood and explained.

V. Conclusion

This paper presented stochastic metrics to evaluate the turbulence rejection capabilities of aircraft under continuous turbulence, which are suitable for gradient-based optimization due to having computationally efficient and accurate analytical derivatives. The formulae presented for the derivatives were validated against a finite difference approximation with excellent agreement. Therefore, these metrics can be incorporated into large-scale MDO problems to access the closed-loop turbulence rejection performance of an aircraft without a detailed controller design.

The proposed analysis is done in the frequency domain and requires linearizing the plant around the trim condition. The use of a linearized analysis, although usual, may not be sufficient in the case of supersonic aircraft at low speeds that have substantial aerodynamics nonlinearities due to the high angles of attack involved and the effects of vortex breakdown. On the other hand, the frequency domain analysis is very efficient for handling stochastic gust models, since it can estimate small probabilities without the need for expensive sampling.

The proposed metrics were used to analyze the SCALOS aircraft. To design the sensitivity function, a minimization problem of the sum of the probabilities of exceeding the limits of glideslope deviation, angle of attack, elevator deflection and elevator deflection rate was introduced and solved. The resulting design suffers from the high elevator deflection needed to trim the vehicle. The probability of elevator saturation is high (12%) and this prevents the optimizer from increasing the bandwidth of the control system, which would provide for better tracking of the glideslope—the probability of exceeding the maximum glideslope deviation is of 4%, as is the probability of exceeding the maximum angle of attack. Redesigning the aircraft to increase longitudinal control authority would help improve these metrics.

Finally, this work demonstrated the feasibility of incorporating controller-agnostic design metrics into MDO for evaluating the capability of a design to reject stochastic disturbances in closed-loop, which should help bring more considerations is the early phases of the design cycle. For future work, more representative and larger models should be tested to demonstrate the relevance and scalability of the proposed metrics.

Acknowledgments

Support by NASA under the Commercial Supersonics Technology (CST) project with Sarah Langston as the NASA technical grant monitor is gratefully acknowledged. Opinions, interpretations, conclusions, and recommendations are those of the authors and are not necessarily endorsed by the United States Government.

References

[1] "2022 Safety Report," Tech. rep., Flight Safety Foundation, Mar. 2023.

[2] Park, M. A., and Carter, M. B., "Nearfield Summary and Analysis of the Third AIAA Sonic Boom Prediction Workshop C608 Low Boom Demonstrator," *AIAA Scitech 2021 Forum*, American Institute of Aeronautics and Astronautics, 2021. doi:10.2514/6.2021-0345.

[3] Rodgers, E., *Foresight, Strategy and Futures Studies for Defense and Security*, Springer, 2023, Chap. NASA Strategy for Technology Development. URL `https://ntrs.nasa.gov/citations/20230000995`.

[4] "NASA Quesst," `https://www.nasa.gov/mission/quesst/`, 2023. Accessed: November 27, 2023.

[5] Fuller, J. R., "Evolution of airplane gust loads design requirements," *Journal of Aircraft*, Vol. 32, No. 2, 1995, pp. 235–246. doi:10.2514/3.46709.

[6] W., L. H., "On the Application of Statistical Concepts to the Buffeting Problem," *Journal of the Aeronautical Sciences*, Vol. 19, No. 12, 1952, pp. 793–800. doi:10.2514/8.2491.

[7] Diederich, F. W., and Drischler, J. A., "Effect of spanwise variations in gust intensity on the lift due to atmospheric turbulence," Tech. rep., NACA, Apr. 1957. TN 3920.

[8] Kaimal, J. C., Wyngaard, J. C., Izumi, Y., and Coté, O. R., "Spectral characteristics of surface-layer turbulence," *Quarterly Journal of the Royal Meteorological Society*, Vol. 98, No. 417, 1972, pp. 563–589. doi:10.1002/qj.49709841707.

[9] Mann, J., "The spatial structure of neutral atmospheric surface-layer turbulence," *Journal of Fluid Mechanics*, Vol. 273, 1994, pp. 141–168. doi:10.1017/s0022112094001886.

[10] Hoblit, F. M., *Gust loads on aircraft: concepts and applications*, AIAA, 1988.

[11] Deskos, G., del Carre, A., and Palacios, R., "Assessment of low-altitude atmospheric turbulence models for aircraft aeroelasticity," *Journal of Fluids and Structures*, Vol. 95, 2020, p. 102981. doi:10.1016/j.jfluidstructs.2020.102981.

[12] Porté-Agel, F., Meneveau, C., and Parlange, M. B., "A scale-dependent dynamic model for large-eddy simulation: application to a neutral atmospheric boundary layer," *Journal of Fluid Mechanics*, Vol. 415, 2000, pp. 261–284. doi:10.1017/s0022112000008776.

[13] Bou-Zeid, E., Meneveau, C., and Parlange, M., "A scale-dependent Lagrangian dynamic model for large eddy simulation of complex turbulent flows," *Physics of Fluids*, Vol. 17, No. 2, 2005, p. 025105. doi:10.1063/1.1839152.

[14] Deskos, G., Laizet, S., and Palacios, R., "WInc3D: A novel framework for turbulence-resolving simulations of wind farm wake interactions," *Wind Energy*, Vol. 23, No. 3, 2020, pp. 779–794. doi:10.1002/we.2458.

[15] Geletu, A., Klöppel, M., Zhang, H., and Li, P., "Advances and applications of chance-constrained approaches to systems optimisation under uncertainty," *International Journal of Systems Science*, Vol. 44, No. 7, 2013, pp. 1209–1232. doi:10.1080/00207721.2012.670310.

[16] Gray, R. M., *Probability, Random Processes, and Ergodic Properties*, Springer US, 2009. doi:10.1007/978-1-4419-1090-5.

[17] Leishman, J. G., *Principles of Helicopter Aerodynamics*, 2nd ed., Cambridge University Press, 2006.

[18] Kac, M., "On the average number of real roots of a random algebraic equation," *Bulletin of the American Mathematical Society*, Vol. 49, No. 4, 1943, pp. 314–320. doi:10.1090/s0002-9904-1943-07912-8.

[19] Rice, S. O., "Mathematical Analysis of Random Noise," *Bell System Technical Journal*, Vol. 24, No. 1, 1945, pp. 46–156. doi:10.1002/j.1538-7305.1945.tb00453.x.

[20] Leadbetter, M. R., Lindgren, G., and Rootzén, H., *Extremes and Related Properties of Random Sequences and Processes*, 1st ed., Springer-Verlag, New York, 1983. doi:10.1007/978-1-4612-5449-2.

[21] Richardson, J. R., Atkins, E. M., Kabamba, P. T., and Girard, A. R., "Envelopes for Flight Through Stochastic Gusts," *Journal of Guidance, Control, and Dynamics*, Vol. 36, No. 5, 2013, pp. 1464–1476. doi:10.2514/1.57849.

[22] Richardson, J. R., Kabamba, P. T., Atkins, E. M., and Girard, A. R., "Safety Margins for Flight Through Stochastic Gusts," *Journal of Guidance, Control, and Dynamics*, Vol. 37, No. 6, 2014, pp. 2026–2030. doi:10.2514/1.g000299.

[23] Garcia-Sanz, M., "Control Co-Design: An engineering game changer," *Advanced Control for Applications*, Vol. 1, No. 1, 2019, p. e18. doi:https://doi.org/10.1002/adc2.18, e18 ADC2-19-0039.

[24] Steinert, A., Steffensen, R., Gierszewski, D., Speckmaier, M., Holzapfel, F., Schmoldt, R., Demmler, F., Schell, U., Ornigg, M., and Koop, M., "Experimental Results of Flight Test Based Gain Tuning," *AIAA SCITECH 2022 Forum*, American Institute of Aeronautics and Astronautics, 2022. doi:10.2514/6.2022-2296.

[25] Sobieszczanski-Sobieski, J., "Multidisciplinary Design Optimization: An Emerging New Engineering Discipline," *Advances in Structural Optimization*, edited by J. Herskovits, Springer Netherlands, Dordrecht, 1995, pp. 483–496. doi:10.1007/978-94-011-0453-1_14.

[26] Hunten, K., Zink, S., Flansburg, B., and Engelstad, S., "A Systems MDO Approach for an Unmanned Aerial Vehicle," *48th AIAA/ASME/ASCE/AHS/ASC Structures, Structural Dynamics, and Materials Conference*, American Institute of Aeronautics and Astronautics, 2007. doi:10.2514/6.2007-1877.

[27] Haghighat, S., Martins, J. R. R. A., and Liu, H. H. T., "Aeroservoelastic Design Optimization of a Flexible Wing," *Journal of Aircraft*, Vol. 49, 2012, pp. 432–443. doi:10.2514/1.C031344.

[28] Xu, J., and Kroo, I., "Aircraft Design with Active Load Alleviation and Natural Laminar Flow," *Journal of Aircraft*, Vol. 51, No. 5, 2014, pp. 1532–1545. doi:10.2514/1.c032402.

[29] Stanford, B., "Optimal Aircraft Control Surface Layouts for Maneuver and Gust Load Alleviation," *AIAA Scitech 2020 Forum*, American Institute of Aeronautics and Astronautics, 2020. doi:10.2514/6.2020-0448.

[30] Vartio, E., Shaw, E., and Vetter, T., "Gust Load Alleviation Flight Control System Design for a SensorCraft Vehicle," *26th AIAA Applied Aerodynamics Conference*, American Institute of Aeronautics and Astronautics, 2008. doi:10.2514/6.2008-7192.

[31] Dillsaver, M., Cesnik, C. E. S., and Kolmanovsky, I., "Gust Load Alleviation Control for Very Flexible Aircraft," *AIAA Atmospheric Flight Mechanics Conference*, American Institute of Aeronautics and Astronautics, 2011. doi:10.2514/6.2011-6368.

[32] Duessler, S., Mylvaganam, T., and Palacios, R., "LQG-based Gust Load Alleviation Systems for Very Flexible Aircraft," *AIAA SCITECH 2023 Forum*, American Institute of Aeronautics and Astronautics, 2023. doi:10.2514/6.2023-2571.

[33] Zeng, J., Moulin, B., de Callafon, R., and Brenner, M. J., "Adaptive Feedforward Control for Gust Load Alleviation," *Journal of Guidance, Control, and Dynamics*, Vol. 33, 2010. doi:10.2514/1.46091.

[34] Haghighat, S., Liu, H. H. T., and Martins, J. R. R. A., "Model-Predictive Gust Load Alleviation Controller for a Highly Flexible Aircraft," *Journal of Guidance, Control, and Dynamics*, Vol. 35, 2012. doi:10.2514/1.57013.

[35] De Freitas Virgilio Pereira, M., "Constrained Control for Load Alleviation in Very Flexible Aircraft," Ph.D. thesis, University of Michigan, 2022. doi:10.7302/6287.

[36] Fournier, H., Massioni, P., Pham, M. T., Bako, L., Vernay, R., and Colombo, M., "Robust Gust Load Alleviation at Different Flight Points and Mass configurations," *AIAA SCITECH 2022 Forum*, American Institute of Aeronautics and Astronautics, 2022. doi:10.2514/6.2022-0285.

[37] Ting, K.-Y., Mesbahi, M., and Livne, E., "Aeroservoelastic Wind Tunnel Evaluation of Preview H_2 and H_∞ Gust Load Alleviation," *Journal of Guidance, Control, and Dynamics*, Vol. 46, No. 11, 2023, pp. 2044–2062. doi:10.2514/1.g007450.

[38] Biannic, J.-M., and Roos, C., "Flare control law design via multi-channel H_∞ synthesis: Illustration on a freely available nonlinear aircraft benchmark," *2015 American Control Conference (ACC)*, IEEE, 2015. doi:10.1109/acc.2015.7170913.

[39] Bahia Monteiro, B., Gray, A. C., Cesnik, C. E. S., Kolmanovsky, I., and Vetrano, F., "Bi-level Multidisciplinary Design Optimization of a Wing Considering Maneuver Load Alleviation and Flutter," *AIAA SCITECH 2023 Forum*, 2023, p. 0728. doi:10.2514/6.2023-0728.

[40] Bahia Monteiro, B., Cesnik, C. E. S., and Kolmanovsky, I., "Gust Load Metrics for Multidisciplinary Design Optimization Considering Fatigue and Active Control," *Royal Aeronautical Society's 8th Aircraft Structural Design Conference*, 2023.

[41] Cunis, T., Kolmanovsky, I., and Cesnik, C. E. S., "Integrating Nonlinear Controllability into a Multidisciplinary Design Process," *Journal of Guidance, Control, and Dynamics*, Vol. 46, No. 6, 2023, pp. 1026–1037. doi:10.2514/1.g007067.

[42] Bertolin, R., Chaves Barbosa, G., Cunis, T., Kolmanovsky, I. V., and Cesnik, C. E. S., "Gust Rejection of a Supersonic Aircraft During Final Approach," *AIAA SCITECH 2022 Forum*, American Institute of Aeronautics and Astronautics, 2022. doi:10.2514/6.2022-2174.

[43] Stein, G., "Respect the unstable," *IEEE Control Systems*, Vol. 23, No. 4, 2003, pp. 12–25. doi:10.1109/mcs.2003.1213600.

[44] Bode, H. W., *Network analysis and feedback amplifier design*, Bell Telephone Laboratories series, D. Van Nostrand, 1945.

[45] Freudenberg, J., and Looze, D., "Right half plane poles and zeros and design tradeoffs in feedback systems," *IEEE Transactions on Automatic Control*, Vol. 30, No. 6, 1985, pp. 555–565. doi:10.1109/tac.1985.1104004.

[46] Seiler, P., Packard, A., and Gahinet, P., "An Introduction to Disk Margins [Lecture Notes]," *IEEE Control Systems Magazine*, Vol. 40, No. 5, 2020, pp. 78–95. doi:10.1109/MCS.2020.3005277.

[47] Martins, J. R. R. A., and Kennedy, G. J., "Enabling large-scale multidisciplinary design optimization through adjoint sensitivity analysis," *Structural and Multidisciplinary Optimization*, Vol. 64, No. 5, 2021, pp. 2959–2974. doi:10.1007/s00158-021-03067-y.

[48] Hwang, J. T., Jain, A. V., and Ha, T. H., "Large-scale multidisciplinary design optimization—review and recommendations," *AIAA Aviation 2019 Forum*, American Institute of Aeronautics and Astronautics, 2019. doi:10.2514/6.2019-3106.

[49] Livne, E., "Supersonic Configurations at Low Speeds (SCALOS): The Incremental Effects of Configuration Variations and Model Regression Studies," *AIAA SCITECH 2023 Forum*, American Institute of Aeronautics and Astronautics, 2023. doi:10.2514/6.2023-0230.

[50] Livne, E., "Supersonic Configurations at Low Speeds (SCALOS): CFD Aided Wind Tunnel Data Corrections," *AIAA SCITECH 2023 Forum*, American Institute of Aeronautics and Astronautics, 2023. doi:10.2514/6.2023-0231.

[51] Ting, K.-Y., Mavriplis, N., Soltani, R. M., Nelson, C. P., Livne, E., of Washington, U., Seattle, and WA, "Supersonic Configurations at Low Speeds (SCALOS): The Aerodynamic Effects of Control Surfaces," *AIAA SCITECH 2023 Forum*, American Institute of Aeronautics and Astronautics, 2023. doi:10.2514/6.2023-0229.

[52] Mavriplis, N., Ting, K.-Y., Moustafa, A., Hill, C., Soltani, R., Nelson, C. P., and Livne, E., "Supersonic Configurations at Low Speeds (SCALOS): Test / Simulation Correlation Studies," *AIAA SCITECH 2022 Forum*, American Institute of Aeronautics and Astronautics, 2022. doi:10.2514/6.2022-1801.

[53] Nelson, C. P., Ting, K.-Y., Mavriplis, N., Soltani, R., and Livne, E., "Supersonic Configurations at Low Speeds (SCALOS): Project Background and Progress at University of Washington," *AIAA SCITECH 2022 Forum*, American Institute of Aeronautics and Astronautics, 2022. doi:10.2514/6.2022-1803.

[54] Ting, K.-Y., Mavriplis, N., Soltani, R., Nelson, C. P., and Livne, E., "Supersonic Configurations at Low Speeds (SCALOS): Model Geometry and Aerodynamic Results," *AIAA SCITECH 2022 Forum*, American Institute of Aeronautics and Astronautics, 2022. doi:10.2514/6.2022-1800.

[55] Guimarães, T. A., Cesnik, C. E. S., and Kolmanovsky, I., "Low Speed Aerodynamic Modeling for Control-related Considerations in Supersonic Aircraft Design," *AIAA Aviation 2021 Forum*, American Institute of Aeronautics and Astronautics, 2021. doi:10.2514/6.2021-2531.

[56] Stanford, B. K., "Gradient-Based Aeroservoelastic Optimization with Static Output Feedback," *Journal of Guidance, Control, and Dynamics*, Vol. 42, No. 10, 2019, pp. 2314–2318. doi:10.2514/1.g004373.

[57] Magnus, J. R., and Neudecker, H., *Matrix Differential Calculus with Applications in Statistics and Econometrics*, 3rd ed., Wiley & Sons, Limited, John, 2019. doi:10.1002/9781119541219.

[58] Guimarães, T. A., Cesnik, C. E. S., and Kolmanovsky, I., "Flexibility Assessment of the Aeroelastic-flight-dynamic Behavior for Supersonic Aircraft," *AIAA SCITECH 2023 Forum*, American Institute of Aeronautics and Astronautics, 2023. doi:10.2514/6.2023-0417.

[59] Stevens, B. L., Lewis, F. L., and Johnson, E. N., *Aircraft Control and Simulation Dynamics, Controls Design, and Autonomous Systems*, 3rd ed., Wiley & Sons, Incorporated, John, 2015.

[60] Guimarães, T. A., Cesnik, C. E. S., and Kolmanovsky, I., "Unsteady Vortex Lattice Linearization and Sensitivity Analyses for Control Models in Supersonic Aircraft Design," *AIAA SCITECH 2023 Forum*, American Institute of Aeronautics and Astronautics, 2023. doi:10.2514/6.2023-0416.

[61] Skogestad, S., and Postlethwaite, I., *Multivariable Feedback Control Analysis and Design*, Wiley & Sons, Limited, John, 2005.

[62] Gray, J. S., Hwang, J. T., Martins, J. R. R. A., Moore, K. T., and Naylor, B. A., "OpenMDAO: An Open-Source Framework for Multidisciplinary Design, Analysis, and Optimization," *Structural and Multidisciplinary Optimization*, Vol. 59, 2019, pp. 1075–1104. doi:10.1007/s00158-019-02211-z.

[63] Kraft, D., "A software package for sequential quadratic programming," *Forschungsbericht- Deutsche Forschungs- und Versuchsanstalt fur Luft- und Raumfahrt*, 1988.